

An insight into parameter identifiability issues in the Carreau-Yasuda model: A novel rheological formulation for shear-thinning non-Newtonian inelastic fluids

Gianluca Santesarti^{a,*}, Michele Marino^a, Francesco Viola^b,
Roberto Verzicco^{b,c,d}, Giuseppe Vairo^a

^a*University of Rome Tor Vergata, Department of Civil Engineering and Computer Science Engineering, 00133 Rome, Italy*

^b*Gran Sasso Science Institute, L'Aquila, 67100, Italy*

^c*University of Rome Tor Vergata, Department of Industrial Engineering, 00133 Rome, Italy*

^d*Physics of Fluids Group, Max Planck Center for Complex Fluid Dynamics, MESA+ Institute and J. M. Burgers Centre for Fluid Dynamics, University of Twente, P.O. Box 217, 7500AE Enschede, Netherlands*

Abstract

The Carreau-Yasuda rheological model is widely employed in both research and industrial applications to describe the shear-thinning behaviour of non-Newtonian inelastic fluids. However, its calibration against experimental data is often affected by intrinsic identifiability issues, which can lead to misleading physical interpretations of model parameters and unreliable flow predictions. In this paper, starting from the analysis of the identifiability challenges associated with the Carreau-Yasuda model, a novel rheological formulation for shear-thinning non-Newtonian inelastic fluids is proposed. Analytical results and exemplary numerical case studies demonstrate that the proposed formulation is based on physically meaningful model parameters, whose identifiability is not compromised by the key limitations of the Carreau-Yasuda model. Moreover, the new approach allows for effective parameter estimation through a straightforward direct identification strategy, eliminating the need for inverse calibration procedures based on optimization techniques.

*Corresponding author

Email addresses: santesarti@ing.uniroma2.it (Gianluca Santesarti),
m.marino@ing.uniroma2.it (Michele Marino), francesco.viola@gssi.it (Francesco Viola),
verzicco@uniroma2.it (Roberto Verzicco), vairo@ing.uniroma2.it (Giuseppe Vairo)

Keywords: non-Newtonian inelastic fluids; shear-thinning fluids; rheological modeling; parameter identifiability properties; Carreau-Yasuda model.

1. Introduction

Fluids used in a wide range of advanced applications exhibit a complex non-Newtonian and non-linear rheological behaviour, characterized by a significant dependence of viscosity on shear rate and/or shear rate history. Typical examples can be found in biomedical engineering [1–3], tribology and industrial processes for the production of lubricants and paints [4], plastic polymer manufacturing [5], food engineering [6]. Among the different types of these complex fluids, in the following reference is made to the class of generalized Newtonian fluids (GNFs), also known as viscous inelastic fluids, that exhibit shear-thinning effects, as for the blood [7, 8]. In this case, the actual shear stress depends on the shear rate at the current time and not upon the history of the deformation rate, and it can be described via a generalized form of the constitutive equation of Newtonian fluids, in which the effective (or apparent) viscosity is a non-linear decreasing function of the shear rate. Specifically, such a non-linear viscosity response generally exhibits small decreasing rates (thereby corresponding to a quasi-Newtonian behaviour) for both low and high shear rate levels, with a significant non-linear transition at intermediate shear rates [4, 5].

Several empirical models can be found in the specialized literature to describe the rheological behaviour of GNFs with a shear-thinning response. The power-law (or Ostwald–de Waele) model [9, 10], defined by two model parameters, expresses the dependence of shear stress on shear rate via a power law. It generally provides a suitable description of the non-linear viscosity behaviour in flow regimes characterized by intermediate shear rates. The Carreau model based on molecular theoretical considerations [11] and the Ellis model [5, 12], are both formulated by introducing three model parameters. They capture the transition from the quasi-Newtonian regime at low shear rates to the highly non-linear behaviour as the shear rate increases. The Cross model [13], de-

fined by four model parameters, allows to capture the transitions between the quasi-Newtonian regime and the non-Newtonian one at both low and high shear rates. The Carreau-Yasuda model [5, 14], also known as the Bird-Cross-Carreau-Yasuda (BCCY) model [15], aims to provide a comprehensive description of the shear-thinning behaviour. In particular, it generalizes and combines both the Cross and Carreau models by introducing the additional Yasuda parameter [14], providing more flexibility in fitting experimental data.

Specifically addressing the BCCY model, it is generally considered to be effective and highly versatile in describing the shear-thinning behaviour of complex fluids. It has been widely adopted in many advanced inherent applications, for instance, hemodynamics [8], plastic manufacturing [16], lubricant production [17], and food processing [18]. However, as highlighted by Gallagher et al. [15] in the context of the dynamics of the hematologic fluid, the BCCY model exhibits intrinsic limitations related to the identifiability of the parameters. Specifically, they found that fitting experimental data using standard non-linear optimization procedures can yield multiple sets of model parameters that provide nearly identical fits to the rheological data. This is due to the presence of large, flat regions in the cost surface around the optimal state. Despite producing almost indistinguishable rheological fits, these parameter variations can lead to significantly different and unreliable flow predictions, making it impossible to draw meaningful conclusions about the physical properties of the fluids. Furthermore, when the BCCY model is used to calibrate piecewise approximations —based on the assumption of a sharp viscosity transition between ideal Newtonian regions (at low and high shear rates) and a power-law behaviour at intermediate shear rates, which could be used to derive analytical solutions [19]— additional inconsistencies in parameter interpretation can arise, as it will be analyzed in the following. These inconsistencies compromise the physical meaning and applicability of the calibrated parameters, further limiting the robustness and reliability of the BCCY model in such scenarios.

In order to contribute to overcoming these identifiability issues, this paper proposes a novel rheological description for shear-thinning inelastic fluids. Com-

comparisons based on analytical closed-form estimates and numerical assessments of calibration performance -considering both direct and inverse identification strategies- highlight the accuracy and reliability of the proposed rheological model. In particular, the results emphasise the clear physical significance of the model parameters that predominantly influence the non-linear response at intermediate shear-rate levels. Moreover, they demonstrate that the proposed formulation effectively mitigates the identifiability issues of the BCCY model, proving to be highly accurate and efficient even with a simple direct calibration, without requiring complex and time-consuming non-linear optimization procedures.

The paper is organized as follows. Section 2 presents a critical analysis of the BCCY formulation. In Section 3, the novel shear-based rheological model is introduced, with analytical developments (complemented by Appendix A) providing theoretical insights into the improved physical interpretability of its parameters compared to those of the BCCY model. Section 4 discusses identifiability performance and numerical comparisons, presenting results of direct and inverse calibration procedures based on available experimental data, and analyzing their impact on a representative flow case study. Finally, concluding remarks are provided in Section 5.

2. An insight into the Carreau-Yasuda model

For incompressible GNFs, the constitutive relationship between the deviatoric stress tensor $\boldsymbol{\tau}$ and the strain-rate tensor \mathbf{E} results in [5]

$$\boldsymbol{\tau}(\dot{\gamma}) = 2\mu(\dot{\gamma}) \mathbf{E} = \mu(\dot{\gamma}) (\nabla \mathbf{v} + \nabla^T \mathbf{v}), \quad (1)$$

where \mathbf{v} is the fluid velocity, ∇ denotes the gradient operator, and $\mu(\dot{\gamma})$ is the effective viscosity depending on the scalar measure $\dot{\gamma}$ of the strain-rate tensor

$$\dot{\gamma} = |\mathbf{2E}| = \sqrt{2 \operatorname{tr}(\mathbf{E}^T \mathbf{E})} = \sqrt{2 I_2}, \quad (2)$$

with I_2 being the second principal trace of the infinitesimal strain-rate tensor [5, 20, 21]. Regarding GNFs that exhibit a shear-thinning behaviour and addressing

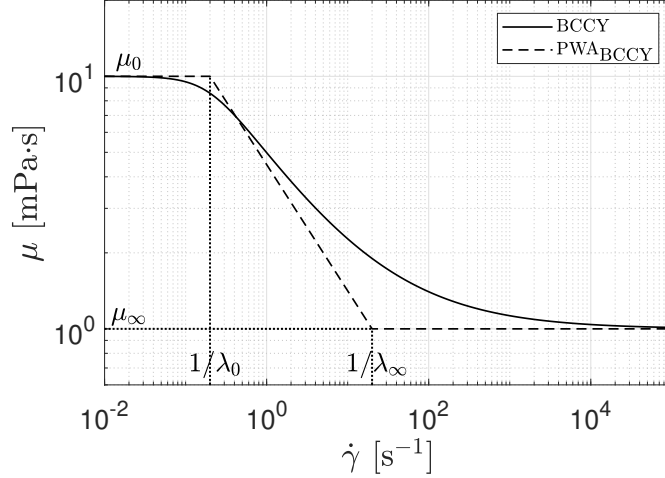


Figure 1: Example case of the Bird-Cross-Carreau-Yasuda (BCCY) shear-thinning description in comparison with a power-law-based piecewise approximation defined in terms of the BCCY model parameters (PWA_{BCCY}), i.e. by considering $N = n$, $\lambda_0 = \lambda$, $\lambda_\infty = \lambda(\mu_\infty/\mu_0)^{1/(1-n)}$, $K = \mu_0\lambda^{n-1}$. Values of model parameters: $\mu_0 = 10 \text{ mPa} \cdot \text{s}$, $\mu_\infty = 1 \text{ mPa} \cdot \text{s}$, $\lambda = 5 \text{ s}$, $n = 0.5$, $a = 2.0$.

the 5-parameters BCCY rheological formulation, the effective viscosity in Eq. (1) may be described as [5, 14]

$$\mu(\dot{\gamma}) = \mu_\infty + \frac{\mu_0 - \mu_\infty}{[1 + (\lambda\dot{\gamma})^a]^{\frac{1-n}{a}}}, \quad (3)$$

where μ_0 and μ_∞ (with $\mu_\infty < \mu_0$) are the zero-shear rate viscosity and the infinity-shear rate viscosity values (measured in $[\text{Pa} \cdot \text{s}]$) attained for very low and very high shear rate levels, respectively, λ (measured in $[\text{s}]$) is a relaxation time constant related to the onset of significant shear-thinning effects, a is a dimensionless strictly-positive model parameter (generally greater than 1), also referred to as the Yasuda parameter [14] which adjusts the transition between quasi-Newtonian regimes and the dominant shear-thinning response, and n is a dimensionless index regulating the corresponding shear-thinning rate, such that $n \in (0, 1)$.

Referring to the example case shown in Fig. 1, the behaviour captured by

the BCCY model is qualitatively consistent with typical experimental observations for many GNFs exhibiting shear-thinning responses [8, 17, 22, 23] and is characterized by:

- a quasi-Newtonian regime at low shear rates (namely, for $\dot{\gamma} \ll 1/\lambda$), associated to a quasi-constant viscosity value $\mu \simeq \mu_0$;
- a strongly non-linear shear-thinning response for intermediate shear rates (i.e., for $\dot{\gamma} > 1/\lambda$);
- a quasi-Newtonian regime at high shear rates (namely, for $\dot{\gamma} \gg 1/\lambda$), associated to the asymptotic viscosity value μ_∞ .

The range of shear rates where the fluid experiences a significant shear-thinning response is usually addressed as power-law region, since it can be effectively described by means of the Ostwald–de Waele power-law relationship [9, 10]. In this case, it is possible to assume that $\tau = K\dot{\gamma}^N$, where τ is a scalar measure of the shear stress, K (measured in $[\text{Pa}\cdot\text{s}^N]$) is the so-called consistency index (with $K > 0$), and N is the dimensionless power-law index. Accordingly, the effective viscosity can be expressed as $\mu(\dot{\gamma}) = \tau/\dot{\gamma} = K\dot{\gamma}^{N-1}$, corresponding to a straight line representation in a log-log graph: $\log_{10} K$ being the intercept of this line with the two axes, and the power-law index N defining the line slope, equal to $N - 1$. Consequently, a shear-thinning response is recovered by prescribing $N \in (0, 1)$. If outside from the power-law region the fluid is approximated as perfectly Newtonian, the viscosity dependency on the shear rate may be described via a power-law-based piecewise approximation (PWA), resulting in

$$\mu(\dot{\gamma}) = \begin{cases} \mu_0 & \text{for } \dot{\gamma} \leq 1/\lambda_0 \\ K\dot{\gamma}^{N-1} & \text{for } 1/\lambda_0 \leq \dot{\gamma} \leq 1/\lambda_\infty \\ \mu_\infty & \text{for } \dot{\gamma} \geq 1/\lambda_\infty \end{cases}, \quad (4)$$

where the continuous but sharp transitions between ideal Newtonian regimes and the shear-thinning region are identified by the time constants λ_0 and λ_∞

(with $\lambda_\infty < \lambda_0$). It is worth observing that the definition of a PWA needs the setting of four model parameters $(\mu_0, \lambda_0, N, \lambda_\infty)$ that, since the continuity requirement at $\dot{\gamma} = 1/\lambda_0$ and $\dot{\gamma} = 1/\lambda_\infty$, have to satisfy the following relationships

$$K = \mu_0 \lambda_0^{N-1} = \mu_\infty \lambda_\infty^{N-1}, \quad \frac{\mu_0}{\mu_\infty} = \left(\frac{\lambda_\infty}{\lambda_0} \right)^{N-1}. \quad (5)$$

A possible point of confusion might be how to introduce a PWA of the BCCY model. To this end, assuming the same values for μ_0 and μ_∞ in both the descriptions, as well as $\lambda_0 = \lambda$, can be clearly considered as consistent choices. Accordingly, for a given value of N , the consistency index K and the time constant λ_∞ directly follow from Eqs. (5). But what about the value for the power-law index N ? A possible direct choice might be to prescribe that the power-law index N coincides with the BCCY model parameter n [24]. Such an assumption is often implicitly enforced as a consequence of (or justifying) the usually-adopted misleading notation, where the same symbol is generally used to indicate both N and n [4, 5, 15, 21]. In the following, the PWA defined by enforcing $N = n$ will be denoted as PWA_{BCCY} .

Referring to the example case introduced in Fig. 1, the comparison between the behaviour predicted by the BCCY model and the corresponding PWA_{BCCY} highlights that:

- the PWA_{BCCY} and the BCCY descriptions are in good agreement in representing the onset of the non-linear shear-thinning response at $\dot{\gamma} \simeq 1/\lambda$;
- for $\dot{\gamma} > 1/\lambda$, the PWA_{BCCY} exhibits a slope that significantly differs from the local BCCY slope across much of the power-law region;
- the non-linear shear-thinning regime described by the BCCY model extends well beyond $\dot{\gamma} = 1/\lambda_\infty$, where the PWA_{BCCY} reaches the lower-bound viscosity value μ_∞ .

The discrepancies revealed between BCCY and PWA_{BCCY} stem from the fact that the BCCY model parameter n in Eq. (3) does not directly correspond to the power-law index N used in the power-law description. Consequently,

when experimental data are fitted by using the BCCY model, the fitting value for n should not be considered as representative of the power-law index N . Similarly, if the experimental shear-thinning regime is fitted by using the Ostwald–de Waele power-law relationship, the BCCY model defined by assuming $n = N$ may not generally provide a good fit, as specifically addressed in Section 4.

This observation is formally supported by calculating the local slope $\mathcal{S}_{\text{BCCY}}$ of the BCCY model in a log-log representation and normalized with respect to the power-law slope $(N - 1)$. In detail, by referring to Eq. (3), it results in

$$\begin{aligned} \mathcal{S}_{\text{BCCY}} &= \frac{1}{N - 1} \frac{d(\log_{10} \mu)}{d(\log_{10} \dot{\gamma})} \\ &= \frac{n - 1}{N - 1} \frac{(\mu_0 - \mu_\infty)(\lambda \dot{\gamma})^a}{\mu_\infty [1 + (\lambda \dot{\gamma})^a]^{1+\beta} + (\mu_0 - \mu_\infty) [1 + (\lambda \dot{\gamma})^a]}, \end{aligned} \quad (6)$$

where $\beta = \left(\frac{1-n}{a}\right) \in (0, 1)$. It is simple to prove that Eq. (6) specialized to the case $n = N$ implies the following inequality (see Appendix A)

$$0 < \mathcal{S}_{\text{BCCY}}|_{n=N} < \frac{1 - \mu_\infty/\mu_0}{1 + \mu_\infty/\mu_0 [(1 + \beta)^{1+\beta}/\beta^\beta - 1]} \equiv \mathcal{U} < 1. \quad (7)$$

As a result, the dimensionless upper bound \mathcal{U} decreases as the ratio μ_∞/μ_0 increases, becoming significantly smaller than one within the admissible range of β . This is clearly illustrated in Fig. 2, where \mathcal{U} is plotted against β for different values of the ratio μ_∞/μ_0 . For completeness and referring to the example case addressed in Fig. 1, the normalized BCCY slope $\mathcal{S}_{\text{BCCY}}|_{N=n}$ introduced in Eq. (6) is also shown, revealing that the discrepancy between the local BCCY slope and the power-law one is always greater than 23%, resulting $\mathcal{S}_{\text{BCCY}}|_{n=N} \leq 0.77 < \bar{\mathcal{U}} \simeq 0.83$, $\bar{\mathcal{U}}$ being the corresponding value of \mathcal{U} .

Therefore, the local slope of the BCCY-based behaviour in a log-log representation does not accurately represent the slope of a power-law description based on the BCCY model parameters, except in the limiting case $\mu_\infty/\mu_0 \rightarrow 0^+$. In particular, the indices n in Eq. (3) and N in Eq. (4) have different meanings, and assuming the same value for them is not consistent. This issue can lead to a misleading physical interpretation of results obtained using the BCCY model

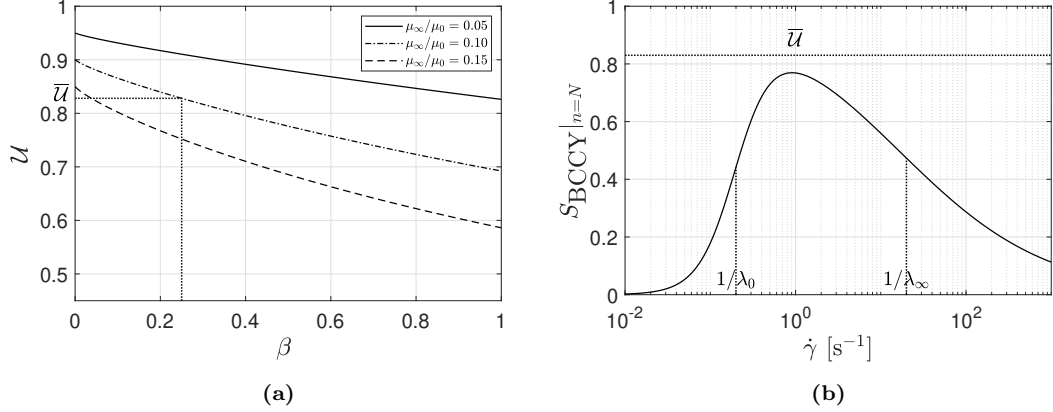


Figure 2: Case $n = N$. (a) Upper bound U introduced in Eq. (7) versus $\beta = (1 - n)/a$ and for different values of the ratio μ_∞/μ_0 . The quantity \bar{U} identifies the value of U corresponding to the example case introduced in Fig. 1 (i.e., for $\beta = 0.25$ and $\mu_\infty/\mu_0 = 0.1$). (b) Shear rate dependency of the normalized BCCY slope $S_{\text{BCCY}}|_{n=N}$ for the example case in Fig. 1.

and may pose a significant challenge for BCCY model parameter identifiability when combined with power-law approximations.

3. A novel shear-based rheological description

In order to overcome the issues associated to the BCCY model and discussed before, a novel rheological description is herein proposed.

The rationale arises from the observation that the viscosity function $\mu(\dot{\gamma})$ in GNFs can be thought as the transfer function between the shear stress scalar measure τ and the applied shear rate $\dot{\gamma}$, the corresponding PWA being the asymptotic description of the Bode-like diagram. Such a transfer function, in agreement with both the previously-recalled physical evidence for shear-thinning inelastic fluids and basic concepts of the control theory, has to be characterized by the static gain μ_0 , and by the presence of both a pole and a zero, each with a multiplicity of one. Specifically, the pole corresponds to the shear rate level $\dot{\gamma}_0 = 1/\lambda_0$, which marks the decrease onset of μ from μ_0 ; the zero is associated to

the shear rate level $\dot{\gamma}_\infty = 1/\lambda_\infty$ beyond which μ stabilizes towards the constant value μ_∞ . Accordingly, the following rheological model is proposed:

$$\mu(\dot{\gamma}) = \mu_0 \left[\frac{1 + (\lambda_\infty \dot{\gamma})^\alpha}{1 + (\lambda_0 \dot{\gamma})^\alpha} \right]^{\frac{1-\eta}{\alpha}}. \quad (8)$$

This description involves five parameters: μ_0 , λ_0 , λ_∞ , and the positive dimensionless quantities α and η , which have meanings formally equivalent to those of a and n , respectively, in Eq. (3). Thereby, when $\lambda_\infty < \lambda_0$ and $\alpha > 1$, a shear-thinning behaviour is obtained if $\eta \in (0, 1)$.

It is worth noticing that, with respect to the BCCY model, the rheological description in Eq. (8) emphasises the role of the time constant λ_∞ as an independent parameter instead of μ_∞ , this latter simply resulting for $\dot{\gamma} \rightarrow +\infty$ from

$$\mu_\infty = \mu_0 \left(\frac{\lambda_\infty}{\lambda_0} \right)^{1-\eta}. \quad (9)$$

In other words, dominant features of the shear-thinning response are assumed to be associated to the shear rate levels $\dot{\gamma}_0 = 1/\lambda_0$ and $\dot{\gamma}_\infty = 1/\lambda_\infty$, that identify the shear rate range in which the highly non-Newtonian response occurs, rather than the asymptotic viscosity value associated to the quasi-Newtonian regime. For this reason the rheological description in Eq. (8) will be denoted in the following as shear rate-based model (SRB).

The proposed model is able to recover two other possible rheological shear-thinning responses:

- In the limit for $\lambda_\infty \rightarrow 0^+$, Eq. (8) reduces to

$$\mu(\dot{\gamma}) = \frac{\mu_0}{[1 + (\lambda_0 \dot{\gamma})^\alpha]^{\frac{1-\eta}{\alpha}}}, \quad (10)$$

that corresponds to the Yasuda model [14], or equivalently to the limit condition associated to the BCCY model for $\mu_\infty \rightarrow 0^+$. This response is representative of a quasi-Newtonian regime characterized by $\mu \simeq \mu_0$ for small shear rates (i.e., for $\dot{\gamma} < 1/\lambda_0$), followed by an indefinite shear-thinning behaviour for any value of the shear rate greater than $1/\lambda_0$.

- In the limit for $\lambda_0 \rightarrow +\infty$, and accounting for Eq. (9), Eq. (8) reduces to

$$\mu(\dot{\gamma}) = \frac{K}{\dot{\gamma}^{1-\eta}} [1 + (\lambda_\infty \dot{\gamma})^\alpha]^{\frac{(1-\eta)}{\alpha}}, \quad (11)$$

with $K = \mu_\infty \lambda_\infty^{\eta-1}$, which describes a shear-thinning behaviour for shear rates lower than $1/\lambda_\infty$ (with a viscosity singularity at $\dot{\gamma} = 0$), followed by a quasi-Newtonian regime characterized by $\mu \simeq \mu_\infty$ for $\dot{\gamma} > 1/\lambda_\infty$.

It is important to emphasise that the model parameter η introduced in Eq. (8) furnishes, in comparison with n in the BCCY description, a more effective representation of the power-law index N associated with a SRB-based PWA. As a matter of fact, the SRB local slope \mathcal{S}_{SRB} , in a log-log representation and normalized with respect to the power-law slope $(N - 1)$, is

$$\begin{aligned} \mathcal{S}_{\text{SRB}} &= \frac{1}{N-1} \frac{d(\log_{10} \mu)}{d(\log_{10} \dot{\gamma})} \\ &= \frac{\eta-1}{N-1} \frac{\dot{\gamma}^a (\lambda_0^a - \lambda_\infty^a)}{[1 + (\lambda_0 \dot{\gamma})^a][1 + (\lambda_\infty \dot{\gamma})^a]}. \end{aligned} \quad (12)$$

In order to perform a consistent comparison among the BCCY, PWA and SRB descriptions, from now on μ_0 and μ_∞ are assumed to have the same values in all the models, and the other parameters are assumed to satisfy the following consistency conditions (see Eq. (9)): $\alpha = a$, $\lambda_0 = \lambda$, $\lambda_\infty = \lambda_0(\mu_\infty/\mu_0)^{1/(1-\eta)}$, $\eta = n = N$. In this case, it can be shown that (see Appendix A)

$$0 < \mathcal{S}_{\text{BCCY}} < \mathcal{S}_{\text{SRB}} < (\mathcal{S}_{\text{SRB}})_{\text{max}} < 1 \quad \text{for} \quad \frac{1}{\lambda_0} < \dot{\gamma} < \frac{1}{\lambda_\infty}, \quad (13)$$

where

$$(\mathcal{S}_{\text{SRB}})_{\text{max}} = \frac{\lambda_0^{a/2} - \lambda_\infty^{a/2}}{\lambda_0^{a/2} + \lambda_\infty^{a/2}} \quad (14)$$

is the maximum value of the shear rate function \mathcal{S}_{SRB} attained at $\dot{\gamma}_{\text{max}} = (\lambda_0 \lambda_\infty)^{-a/2} \in (1/\lambda_0, 1/\lambda_\infty)$.

In this case and for different choices of model parameters, Fig. 3 clearly highlights that the SRB slope is significantly closer to the power-law one within the overall shear-thinning regime than the BCCY case. Accordingly, the model

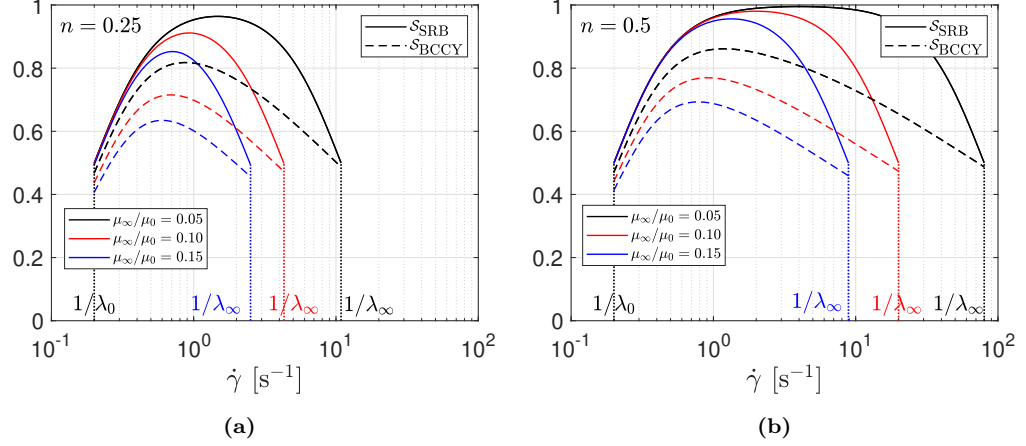


Figure 3: Shear-rate dependency of local normalized slopes $\mathcal{S}_{\text{BCCY}}$ (dashed lines) and \mathcal{S}_{SRB} (continuous lines) introduced in Eqs. (6) and (12), respectively. Values of model parameters: $\alpha = a = 2$, $\lambda_0 = \lambda = 5$ s, $\lambda_\infty = \lambda_0(\mu_\infty/\mu_0)^{1/(1-\eta)}$, $\eta = n = N$. (a) Case $n = 0.25$. (b) Case $n = 0.5$.

parameter η introduced in the SRB description is expected to be much more representative of the power-law index associated to a power-law-based approximation than the corresponding parameter n appearing in the BCCY model. This is clearly confirmed by analyzing Fig. 4 where, for different values of $\eta = N$, the non-linear responses experienced by considering PWA and SRB descriptions are in a very good agreement each other, whereas the BCCY model defined by considering $n = N$ significantly deviates from them within the shear-thinning region.

4. Model parameter identifiability and flow description

To highlight the parameter identifiability issues associated with the BCCY model and to demonstrate the superior identifiability performance of the proposed SRB description, direct and inverse calibration procedures based on available experimental measurements are presented. Specifically, reference is made to the experimental viscosity data obtained by Colosi et al. [25] for a cell-laden

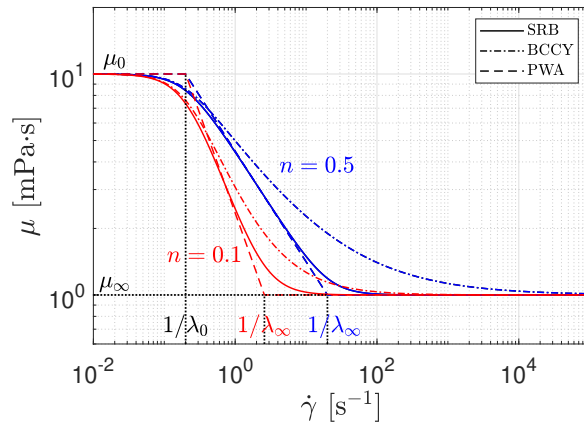


Figure 4: Shear-thinning response associated to SRB, BCCY and PWA descriptions and by assuming $\eta = n = N$, $\lambda_0 = \lambda$, $\lambda_\infty = \lambda_0(\mu_\infty/\mu_0)^{1/(1-n)}$, $K = \mu_0\lambda_0^{\eta-1}$. Values of model parameters: $\mu_0 = 10 \text{ mPa} \cdot \text{s}$, $\mu_\infty = 1 \text{ mPa} \cdot \text{s}$, $\lambda_0 = 5 \text{ s}$, $a = 2$, $n = 0.5$ (blue), $n = 0.1$ (red).

hydrogel, which exhibits a typical shear-thinning response. For the sake of simplicity, the model parameters α (for SRB) and a (for BCCY) are assumed to be equal, and characterized by the a-priori fixed value $\alpha = a = 2$ which gives good fits for many polymeric fluids and melts [5, 21]. Finally, the performance of both rheological models in capturing the flow properties of a representative shear-thinning fluid is briefly discussed. Specifically, in order to clearly highlight the descriptive capability of the models, independent of possible effects related to the specificity of the application, reference is made to the simple case of a steady flow in a cylindrical channel.

4.1. Direct model calibration from experimental data

Parameters for both the BCCY and the SRB models are initially identified by using a direct calibration procedure from experimental data, without employing iterative approaches. Specifically, Fig. 5 shows the experimental data (represented by square symbols) as represented via a log-log plot in the plane $(\dot{\gamma}, \mu)$. The adopted direct calibration procedure is defined on the following steps:

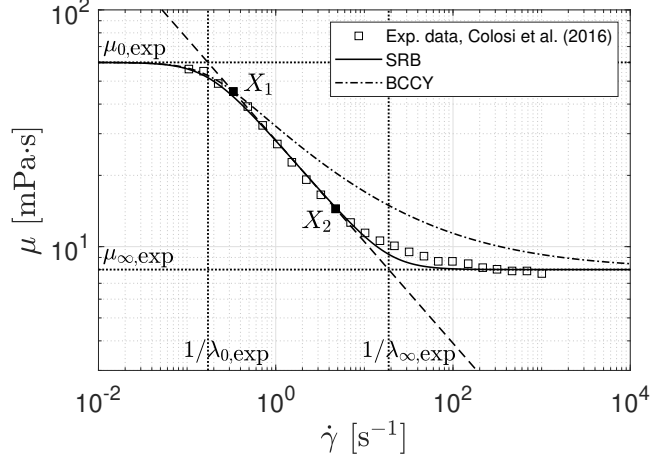


Figure 5: Direct calibration procedure based on a straightforward heuristic visual fitting of the experimental data reported in [25]. Comparison between the corresponding SRB and BCCY rheological descriptions, defined by the experimentally-derived model parameters summarized in Table 1 ($a = \alpha = 2$, $n = \eta = N_{\text{exp}}$, $\lambda = \lambda_{0,\text{exp}}$).

- Identification of asymptotic viscosity values. The experimental estimates for the asymptotic viscosity values, denoted as $\mu_{0,\text{exp}}$ and $\mu_{\infty,\text{exp}}$ are assumed to approximate the largest and smallest viscosity experimental measurements, respectively. In Fig. 5, $\mu_{0,\text{exp}}$ and $\mu_{\infty,\text{exp}}$ are represented by horizontal dot lines.
- Identification of the power-law region. The power-law region is identified by considering the portion of the experimental data that in the log-log plot exhibits a linear trend. In the case under consideration (Fig. 5), such a linear trend is described through the straight dashed line passing through the experimental data points $X_1 \equiv (\dot{\gamma}_1, \mu_1)$ and $X_2 \equiv (\dot{\gamma}_2, \mu_2)$. Accordingly, the experimentally-deduced power-law parameters, namely the consistency index K and the dimensionless power-law index N , straightly result from

$$K_{\text{exp}}^* = \frac{\mu_1^* \dot{\gamma}_2^* - \mu_2^* \dot{\gamma}_1^*}{\dot{\gamma}_2^* - \dot{\gamma}_1^*}, \quad N_{\text{exp}} = 1 - \frac{\mu_1^* - \mu_2^*}{\dot{\gamma}_2^* - \dot{\gamma}_1^*}, \quad (15)$$

where $q^* = \log_{10} q$.

Table 1: Values of model parameters derived through the direct calibration procedure from the experimental data reported in [25].

$\mu_{0,\text{exp}}$	$\mu_{\infty,\text{exp}}$	K_{exp}	N_{exp}	$\lambda_{0,\text{exp}}$	$\lambda_{\infty,\text{exp}}$
[mPa · s]	[mPa · s]	[mPa · s ^N]	[–]	[s]	[s]
60.0	8.0	28.2	0.571	5.812	0.053

- Determination of time constants. Since Eqs. (5), the experimentally-based time constants $\lambda_{0,\text{exp}}$ and $\lambda_{\infty,\text{exp}}$ are determined as follows:

$$\lambda_{0,\text{exp}} = \left(\frac{K_{\text{exp}}}{\mu_{0,\text{exp}}} \right)^{\frac{1}{N_{\text{exp}}-1}}, \quad \lambda_{\infty,\text{exp}} = \left(\frac{K_{\text{exp}}}{\mu_{\infty,\text{exp}}} \right)^{\frac{1}{N_{\text{exp}}-1}}. \quad (16)$$

The inverses of these constants correspond to the shear-rate levels at which the power-law dashed line in Fig. 5 intersects the two horizontal dotted lines representing the asymptotic viscosity values.

The values of model parameters derived from the experimental viscosity data through the described direct calibration procedure are reported in Table 1. Assuming $n = \eta = N_{\text{exp}}$ and $\lambda = \lambda_{0,\text{exp}}$, Fig. 5 represents a comparison between the rheological responses obtained from the BCCY and SRB descriptions. As it clearly appears, the SRB model demonstrates excellent fitting capability, whereas the BCCY model provides a good fit only in the transition region at $\dot{\gamma} \simeq 1/\lambda_{0,\text{exp}}$, failing to accurately capture the experimental behaviour in the power-law region and the transition towards the asymptotic quasi-Newtonian response at $\mu \simeq \mu_{\infty,\text{exp}}$.

Accordingly, the herein-described simple direct calibration procedure provides an effective and accurate SRB-based rheological description. However, it proves insufficient for the BCCY model, which requires a more complex optimization procedure, as discussed in the following.

4.2. Inverse model calibration through an optimization procedure

Model calibration is now performed using an optimization procedure based on the maximum likelihood estimation method [26]. Specifically, the optimiza-

tion problem aims to determine the set of model parameters that minimize the lognormal mean absolute percentage error (LMAPE):

$$\text{LMAPE} = \frac{1}{T} \sum_{i=1}^T \left| \frac{\log f_i}{\log b_i} - 1 \right|, \quad (17)$$

where the logarithm operator is taken to base 10, T is the number of experimental measurements, b_i denotes the i -th measured viscosity value, and f_i represents the corresponding prediction provided by the rheological model.

The coefficient of determination is then given by:

$$R_{\text{LMAPE}}^2 = 1 - \frac{\text{LMAPE}}{\frac{1}{T} \sum_{i=1}^T \left| \frac{\bar{y}_L}{\log b_i} - 1 \right|}, \quad (18)$$

where $\bar{y}_L = (\sum_{i=1}^T \log b_i)/T$ represents the mean logarithmic experimental value. A value of R_{LMAPE}^2 close to one indicates that the rheological model closely fits the experimental data, while a value approaching zero suggests poor model accuracy [26].

As a result of an iterative numerical procedure implemented in the MATLAB environment (R2024b, MathWorks, MA, USA), Table 2 summarizes the optimal parameter values computed for both the BCCY and SRB models. It is worth noting that, in accordance with the considerations presented in Sections 2 and 3, the parameter λ_∞ is not a primary model parameter in the BCCY formulation but is instead derived from Eqs. (5) once μ_0 , μ_∞ , and λ are determined. Conversely, in the SRB model, λ_∞ is treated as a primary parameter, while μ_∞ is derived from Eq. (9).

For completeness, Table 2 also reports the optimal LMAPE values along with the corresponding values for the coefficient of determination R_{LMAPE}^2 .

Specifically, the minimum LMAPE value obtained by the optimization procedure for the SRB model is slightly higher than that of the BCCY model. Consequently, the coefficient of determination R_{LMAPE}^2 for the SRB model is marginally lower than that for the BCCY formulation. This outcome suggests that, when using the computed optimal parameter sets, the BCCY model provides a slightly better fit to the experimental data compared to the SRB model.

Table 2: Inverse calibration of model parameters for SRB and BCCY rheological descriptions performed via an optimization procedure based on the maximum likelihood estimation method. Primary and derived (underlined) fitting values ($a = \alpha = 2$, $n^* = \eta$ and $\lambda^* = \lambda_0$ for SRB; $n^* = n$ and $\lambda^* = \lambda$ for BCCY).

	μ_0	μ_∞	λ^*	λ_∞	n^*	LMAPE	R_{LMAPE}^2
	[mPa · s]	[mPa · s]	[s]	[s]	[-]	[-]	[%]
SRB	60.0	<u>8.14</u>	5.747	0.053	0.573	0.0155	93.1
BCCY	60.1	7.70	3.759	<u>0.209</u>	0.289	0.0034	98.5

Nevertheless, the SRB model still demonstrates very good fitting performance, with $R_{\text{LMAPE}}^2 \simeq 0.93$. This evidence is clearly highlighted in Fig. 6, where the experimental data from Colosi et al. [25] are well fitted by both the SRB and BCCY models calibrated through the numerical optimization.

On the other hand, the comparison between the values summarized in Table 2 and those reported in Table 1 reveals that the BCCY optimal parameters significantly differ from those obtained through the simple direct calibration procedure described in Section 4.1. In contrast, the direct identification procedure, based on a straightforward heuristic visual fitting approach, yields a calibration for the SRB model that closely matches the optimal one numerically obtained via the iterative minimization strategy.

Let the power-law-based piecewise approximations PWA_{SRB} and PWA_{BCCY} be considered (see Eq. (4)), built up with the inverse calibration results associated with the SRB and BCCY descriptions, respectively. As shown in the comparison presented in Fig. 6, PWA_{BCCY} , despite being based on optimal parameters that ensure the best fit for the BCCY description, fails to effectively capture the experimental response. In contrast, PWA_{SRB} exhibits an excellent agreement with the experimental data, accurately reproducing both the power-law behaviour and the transition phases toward quasi-Newtonian regimes.

This result provides further compelling evidence of a critical identifiability issue associated with the BCCY description, arising from the fact that the BCCY model parameter n in Eq. (3) ($n = 0.289$ at the optimality condition)

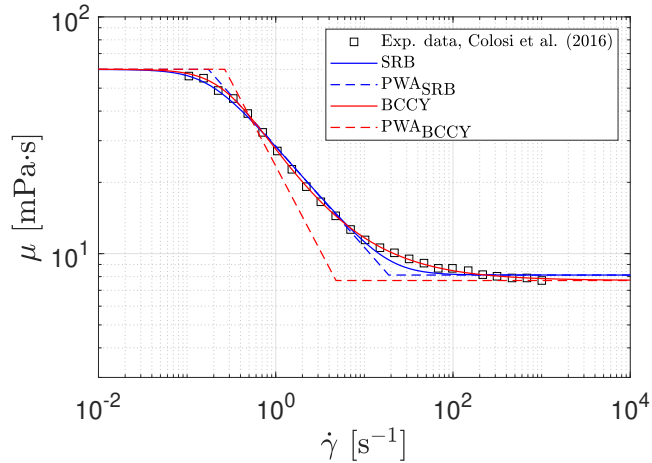


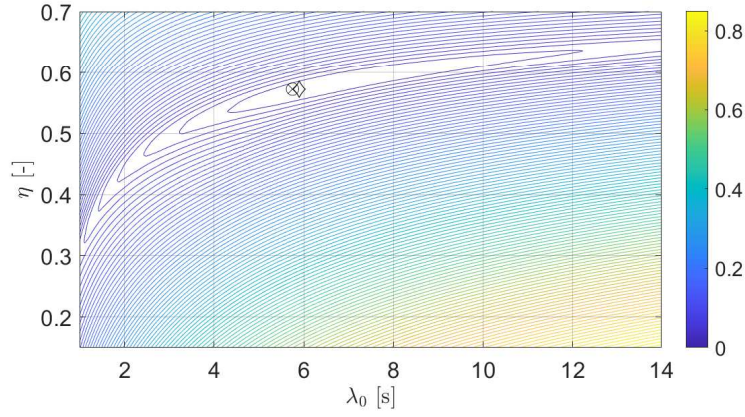
Figure 6: Inverse model calibration through numerical optimization. Comparison of the fitting performance of the SRB and BCCY models, along with their corresponding piecewise approximations (PWA_{SRB} and PWA_{BCCY}). The optimal values of the model parameters are summarized in Table 2.

does not directly correspond to the power-law index N used in the power-law description. Instead, the proposed results confirm that the power-law index N is more accurately represented by the SRB model parameter η in Eq. (8) ($\eta = 0.573$ at the optimality condition).

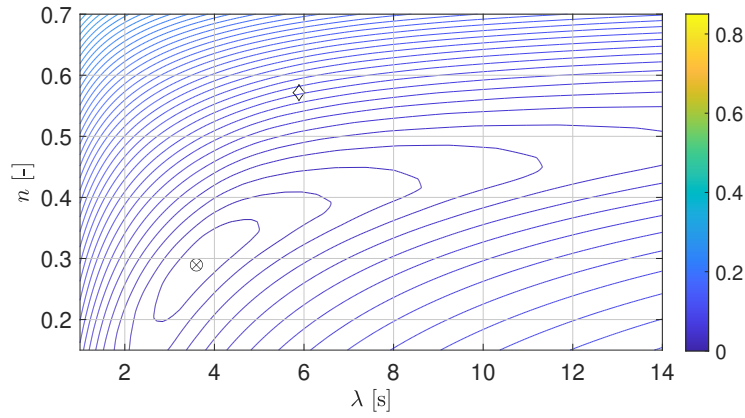
Finally, to demonstrate the greater robustness of the proposed SRB model in terms of identifiability features, particularly in comparison to the BCCY model, the variability of LMAPE associated to deviations of model parameters from the optimality condition is analyzed. For the sake of simplicity, reference is made to λ^* and n^* only ($n^* = \eta$ and $\lambda^* = \lambda_0$ for SRB; $n^* = n$ and $\lambda^* = \lambda$ for BCCY), as these primary parameters play a key role in capturing the onset and evolution of the non-linear shear-thinning response. Specifically, let the likelihood function \mathcal{L} be defined as

$$\mathcal{L}(\lambda^*, n^*) = \text{LMAPE}(\lambda^*, n^*, \hat{\mathcal{P}}), \quad (19)$$

where $\hat{\mathcal{P}}$ denotes the set of primary model parameters complementary to λ^* and n^* , which are held fixed at their optimal values (see Table 2). Figure 7 presents



(a)



(b)

Figure 7: Isolines of the likelihood surface $\mathcal{L}(\lambda^*, n^*)$ introduced in Eq. (19) ($n^* = \eta$ and $\lambda^* = \lambda_0$ for SRB; $n^* = n$ and $\lambda^* = \lambda$ for BCCY). Model parameters different from λ^* and n^* are held fixed and equal to the optimal values summarized in Table 2. (a) SRB model: $\mathcal{L}(\lambda_0, \eta)$; (b) BCCY model: $\mathcal{L}(\lambda, n)$. \otimes : optimality condition computed via the inverse calibration strategy; \diamond : direct calibration state.

the isolines of the likelihood surface $\mathcal{L}(\lambda^*, n^*)$ obtained for the SRB and BCCY descriptions. For completeness, the corresponding optimality conditions and the result of the direct calibration procedure are also indicated.

Once again, it clearly appears that in the case of the SRB model the inverse

and the direct calibration procedures give very close results, differently from the case of the BCCY description. Furthermore, the analysis of the isolines of $\mathcal{L}(\lambda, n)$ obtained for the BCCY model (Fig. 7b) confirms the findings provided by Gallagher et al. [15]. As a matter of fact, the BCCY likelihood surface exhibits a large flat region around the optimality condition. Consequently, significant variations of model parameters λ and n can marginally affect the fitting of the experimental data, but they can lead to very different flow dynamics (as discussed in the following), making these parameters unreliable for inferring the physical properties of the investigated fluid.

By contrast, this identifiability issue is substantially mitigated in the proposed SRB model. The corresponding likelihood surface exhibits steep gradients around the optimal condition, indicating that even small perturbations in λ_0 and η result in significant variations in $\mathcal{L}(\lambda_0, \eta)$. Consequently, minor changes in the primary parameters can noticeably affect the fit performance of the model against the experimental data. This behaviour, combined with the fact that the SRB model can be effectively calibrated through a direct approach, underscores its superior identifiability properties, making it a more effective and robust alternative to the BCCY formulation.

4.3. A representative case of flow description

To further emphasise the previously stated observations regarding the impact of potential identifiability issues on the flow description of generalized Newtonian fluids, reference is made to the simple case of a steady flow in a cylindrical channel involving an exemplary shear-thinning incompressible fluid. This case can be considered representative of an extrusion-based bioprinting process [27–29]. In particular, a cylindrical nozzle is examined, where R denotes the cross-sectional radius and L the axial length (i.e., along the coordinate z). Accordingly, the steady flow is fully described by the following axisymmetric one-dimensional problem [5, 29]:

Table 3: Primary and derived (underlined) fitting values of model parameters, obtained through the inverse calibration procedure and based on synthetic data reported in Fig. 8 ($a = \alpha = 2$, $n^* = \eta$ and $\lambda^* = \lambda_0$ for SRB; $n^* = n$ and $\lambda^* = \lambda$ for BCCY).

	μ_0	μ_∞	λ^*	λ_∞	n^*
	[mPa · s]	[mPa · s]	[s]	[s]	[-]
SRB	60.0	<u>8.14</u>	$9.58 \cdot 10^{-2}$	$8.86 \cdot 10^{-4}$	0.573
BCCY	60.1	7.00	$6.25 \cdot 10^{-2}$	<u>$4.24 \cdot 10^{-3}$</u>	0.300

$$\begin{aligned}
 \frac{1}{r} \frac{d}{dr} \left[r \mu(\dot{\gamma}) \frac{dv_z}{dr} \right] + \frac{\Delta p}{L} &= 0 && \text{for } r \in [0, R] \\
 \frac{dv_z}{dr} &= 0 && \text{at } r = 0 \\
 v_z &= 0 && \text{at } r = R
 \end{aligned} \tag{20}$$

where $\Delta p/L = -dp/dz$ is the constant axial pressure gradient, $v_z = v_z(r)$ is the axial velocity component (the only non-zero component), r is the radial coordinate, and $\dot{\gamma}$ is the scalar shear-rate measure, given by $\dot{\gamma} = |dv_z/dr|$.

The rheological description of the exemplary fluid has been defined considering a set of 50 synthetic data points representing a typical shear-thinning behaviour, as shown in Fig. 8. The model parameters resulting from the numerical inverse calibration procedure introduced in Section 4.2 are summarized in Table 3 for both SRB and BCCY. The corresponding rheological predictions are compared in Fig. 8. Furthermore, Fig. 8 illustrates the rheological predictions of both models when a variation in the primary model parameters n^* and λ^* (that is, n and λ for BCCY, and η and λ_0 for SRB) is introduced with respect to the optimality condition. Specifically, n^* is increased by 15%, while λ^* is reduced by 15%, both relative to their optimal values (see Table 3).

Starting from the fluid rheological response, the steady velocity profile can be computed by solving the problem introduced in Eqs. (20). In particular, assuming $\Delta p/L = 175.0$ Pa/mm and $R = 100 \mu\text{m}$, Fig. 9 depicts the velocity profiles associated with both the optimality conditions and the perturbed ones,

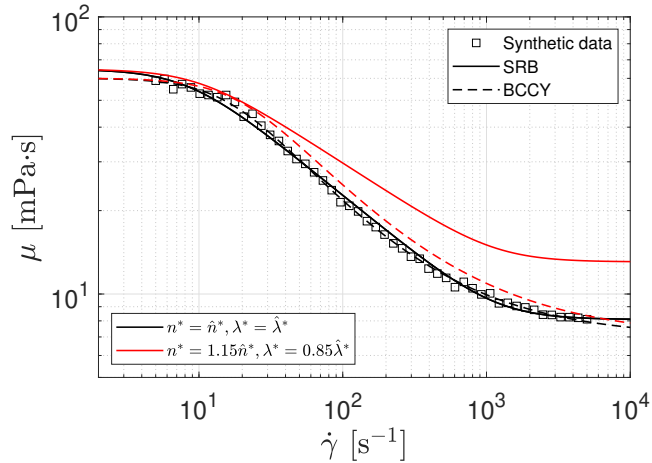


Figure 8: Rheological response of a representative shear-thinning fluid defined by a set of 50 synthetic data points (square symbols). Optimal fittings (black lines) obtained through the inverse calibration procedure for both the SRB (solid line) and BCCY (dashed line) formulations. The optimal model parameter values are summarized in Table 3. Red lines represent the rheological predictions when the primary model parameters n^* and λ^* ($n^* = n$ and $\lambda^* = \lambda$ for BCCY; $n^* = \eta$ and $\lambda^* = \lambda_0$ for SRB) are perturbed with respect to the optimal condition.

computed via a numeric finite-difference scheme. Moreover, Fig. 9 also shows the analytical solutions derived by assuming the fluid response in the cylindrical nozzle as completely described by the Ostwald-de Waele power-law model, that is by considering $\mu(\dot{\gamma}) = K\dot{\gamma}^{N-1}$. In this case, the velocity profile is analytically represented by [5, 29]:

$$v_z(r) = \frac{N}{N+1} \left(\frac{\Delta p}{2LK} \right)^{\frac{1}{N}} \left(R^{\frac{N+1}{N}} - r^{\frac{N+1}{N}} \right), \quad (21)$$

where, accounting for Eq. (5), model parameters K and N are computed via μ_0 , λ^* and $N = n^*$ (with $n^* = \eta$ and $\lambda^* = \lambda_0$ for SRB; $n^* = n$ and $\lambda^* = \lambda$ for BCCY) corresponding to the optimal calibration results (see Table 3).

The proposed results show that:

- The velocity profiles numerically computed using both the SRB and BCCY models under optimal conditions are very similar, with differences of less

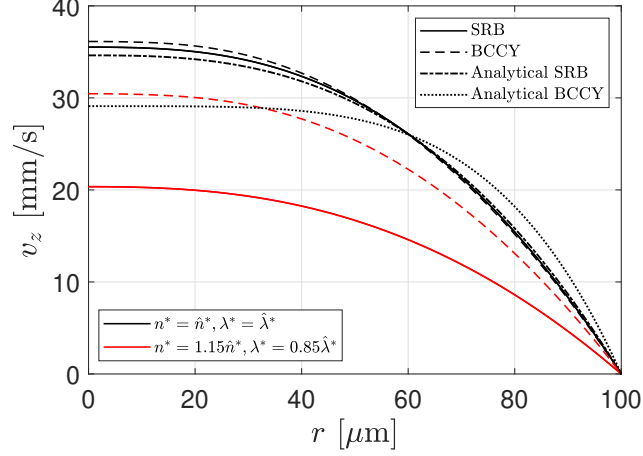


Figure 9: Prediction of velocity profiles for a steady incompressible flow in a cylindrical channel ($\Delta p/L = 175.0$ Pa/mm, $R = 100$ μm) when the rheological shear-thinning response in Fig. 8 is considered. Numerical predictions based on SRB (solid lines) and BCCY (dashed lines) models: comparison between velocity profiles associated with the optimality conditions (black lines) and the perturbed ones (red lines). Power-law-based analytical solution, described by Eq. (21) and obtained via the optimal calibration results for both SRB and BCCY models, is also reported. The optimal model parameter values are summarized in Table 3.

than 2%. Moreover, both models yield nearly the same cross-section average velocity, $\bar{V} \simeq 20$ mm/s.

- When model parameters deviate from their optimal values, the BCCY formulation continues to provide a reasonably accurate rheological description compared to the reference data, unlike the SRB formulation (Fig. 8). Specifically, the maximum deviation between BCCY predictions and the reference data remains below 11%, whereas discrepancies in the SRB-based rheological description can exceed 60%.
- Although significant deviations from the optimal model parameters do not substantially affect the rheological response of the BCCY model, the resulting flow description can differ significantly from the actual one (see Fig. 9). Specifically, considerable discrepancies arise when comparing the

BCCY-based velocity profiles computed using the optimal calibration and the perturbed parameters, with differences exceeding 17% (approximately 14% in the average velocity value). This evidence further confirms the identifiability issue of the BCCY model, as highlighted by Gallagher et al. [15].

- The analytical velocity profile obtained using the Ostwald–de Waele power-law model based on the SRB optimal calibration exhibits excellent agreement with the optimal numerical solutions, with differences lower than 4%. In contrast, the power-law analytical profile derived from the BCCY optimal calibration shows significant discrepancies compared to the optimal numerical solutions, with differences exceeding 17%. Given the values summarized in Table 3, this finding further confirms that the BCCY model parameter n cannot be directly adopted—or straightforwardly identified—within a power-law description. Conversely, the SRB model parameter η is better suited to approximate the power-law index N . Therefore, the SRB formulation effectively overcomes the critical identifiability issues of the BCCY model, enabling a simple and efficient calibration procedure based on a direct approach.

5. Conclusions

The Carreau-Yasuda model (BCCY) is widely used to describe the shear-thinning behaviour of non-Newtonian inelastic fluids in many research and industrial applications. However, its calibration is often affected by intrinsic identifiability issues, leading to misleading interpretations of model parameters and unreliable flow predictions. To address these limitations, this paper proposed a novel rheological formulation specifically designed to mitigate such identifiability challenges.

Comparisons based on analytical arguments and numerical assessments demonstrated that the proposed model relies on physically meaningful parameters, whose identifiability is not compromised by the key issues affecting the Carreau-

Yasuda formulation. Moreover, the new approach allows for effective parameter estimation through a straightforward direct identification strategy, eliminating the need for complex and time-consuming numerical inverse calibration procedures.

The results presented in this study highlight that the novel model not only provides a robust and accurate description of shear-thinning fluids but also ensures improved reliability in flow predictions. By addressing the fundamental shortcomings of the BCCY model, this formulation represents a promising alternative for advanced applications requiring precise rheological characterizations. Future work may extend the analysis to more complex flow conditions and validate the model against a broader set of experimental data.

Acknowledgments

Part of this work was carried out with the support from the Italian National Group for Mathematical Physics GNFM-INdAM.

Michele Marino and Giuseppe Vairo acknowledge financial support by the Italian Ministry of University and Research (MUR) under the National Recovery and Resilience Plan (NRRP), PRIN 2022 program, Project 2022T3SLAZ – CUP E53D23003700006.

Appendix A.

Consistently with symbols defined in Sections 2 and 3, and by assuming $\alpha = a$, $\eta = n = N$, $\lambda = \lambda_0$, let the following notation be introduced

$$x = (\lambda_0 \dot{\gamma})^a, \quad \beta = \frac{1-n}{a}, \quad g = \left(\frac{\lambda_\infty}{\lambda_0} \right)^a, \quad (\text{A.1})$$

so that

$$\mu_\infty/\mu_0 = g^\beta, \quad 0 < \beta < 1, \quad 0 < g < g^\beta < 1. \quad (\text{A.2})$$

Thereby, the shear rate range $1/\lambda_0 \leq \dot{\gamma} \leq 1/\lambda_\infty$, that identifies the shear-thinning region, corresponds to $1 < x < 1/g$. Accordingly, Eqs. (6) and (12)

can be recast as

$$\mathcal{S}_{\text{BCCY}}(x) = \frac{x(1 - g^\beta)}{(1 + x)[(1 - g^\beta) + g^\beta(1 + x)^\beta]} , \quad (\text{A.3})$$

$$\mathcal{S}_{\text{SRB}}(x) = \frac{x(1 - g)}{(1 + x)(1 + gx)} . \quad (\text{A.4})$$

Appendix A.1. Proof of the inequality (7)

For shear rate levels inducing shear-thinning (i.e., for $x > 1$), functions $(1 + x)/x$ and $(1 + x)^{\beta+1}/x$ are both strictly greater than one. Moreover, the latter attains its minimum value $(1 + \beta)^{1+\beta}/\beta^\beta > 1$ at $x = 1/\beta > 1$. As a result, and accounting for relationships (A.2), the following inequality holds

$$\begin{aligned} 0 < \mathcal{S}_{\text{BCCY}}(x) &= \frac{1 - g^\beta}{\frac{1+x}{x}(1 - g^\beta) + \frac{(1+x)^{\beta+1}}{x}g^\beta} \\ &< \frac{1 - g^\beta}{1 + g^\beta \left[\frac{(1+\beta)^{\beta+1}}{\beta^\beta} - 1 \right]} < 1 , \end{aligned} \quad (\text{A.5})$$

that corresponds to the inequality (7).

Appendix A.2. Proof of the inequality (13)

The derivative of Eq. (A.4) with respect to x gives

$$\frac{d\mathcal{S}_{\text{SRB}}}{dx} = \frac{(1 - t)(1 - x^2t)}{(1 + x)^2(1 + xt)^2} , \quad (\text{A.6})$$

resulting in $\text{sgn}(d\mathcal{S}_{\text{SRB}}/dx) = \text{sgn}(1 - x^2t)$. Since the function $(1 - x^2t)$ is strictly decreasing for $x > 1$ and it vanishes for $x = 1/\sqrt{t}$, the corresponding stationary condition for \mathcal{S}_{SRB} corresponds to the maximum value

$$\mathcal{S}_{\text{SRB}} \left(\frac{1}{\sqrt{t}} \right) = (1 - \sqrt{t})/(1 + \sqrt{t}), \quad (\text{A.7})$$

that is the Eq. (14).

In order to prove the inequality (13), let the function $\Delta\mathcal{S}(x) = \mathcal{S}_{\text{SRB}}(x) - \mathcal{S}_{\text{BCCY}}(x)$ be introduced. Since the strict positivity of both the denominators of $\mathcal{S}_{\text{BCCY}}$ and \mathcal{S}_{SRB} when $1 < x < 1/g$, the sign of $\Delta\mathcal{S}$ coincides with the sign of the following continuous function

$$F(x) = (1 - g)[(1 - g^\beta) + g^\beta(1 + x)^\beta] - (1 - g^\beta)(1 + gx) . \quad (\text{A.8})$$

It can be simply shown that the solutions of the equation $F(x) = 0$ are

$$x_1 = -1, \quad x_2 = \frac{1}{g} \left(\frac{1-g}{1-g^\beta} \right)^{\frac{1}{1-\beta}} - 1. \quad (\text{A.9})$$

Moreover, due to inequalities in (A.2), the following condition holds

$$\frac{1-g}{1-g^\beta} > \frac{1-g^2}{1-g^\beta} = \frac{1-g}{1-g^\beta} (1+g) > 1+g > (1+g)^{1-\beta}, \quad (\text{A.10})$$

that straight implies $x_2 > 1/g > 1$.

On the other hand, due to the continuity of $F(x)$ and observing that $F(0) = g^\beta - g > 0$, it results

$$\text{sgn}(F) = \text{sgn}(\Delta\mathcal{S}) = +1 \quad \text{for } 1 < x < \frac{1}{g}, \quad (\text{A.11})$$

that is equivalent to the inequality (13).

References

- [1] B. M. Johnston, P. R. Johnston, S. Corney, D. Kilpatrick, Non-newtonian blood flow in human right coronary arteries: steady state simulations, *Journal of biomechanics* 37 (5) (2004) 709–720.
- [2] P. A. Amorim, M. d’Ávila, R. Anand, P. Moldenaers, P. Van Puyvelde, V. Bloemen, Insights on shear rheology of inks for extrusion-based 3d bioprinting, *Bioprinting* 22 (2021) e00129.
- [3] B. Sauty, G. Santesarti, T. Fleischhammer, P. Lindner, A. Lavrentieva, I. Pepelanova, M. Marino, Enabling technologies for obtaining desired stiffness gradients in gelma hydrogels constructs, *Macromolecular Chemistry and Physics* 223 (2) (2022) 2100326.
- [4] R. P. Chhabra, J. F. Richardson, *Non-Newtonian flow and applied rheology: engineering applications*, Butterworth-Heinemann, 2011.

- [5] R. B. Bird, R. C. Armstrong, O. Hassager, Dynamics of polymeric liquids. Vol. 1: Fluid mechanics, John Wiley and Sons Inc., New York, NY, 1987.
- [6] M. A. Rao, Rheology of fluid and semisolid foods: principles and applications, Springer Science & Business Media, 2010.
- [7] E. M. Cherry, J. K. Eaton, Shear thinning effects on blood flow in straight and curved tubes, *Physics of Fluids* 25 (7) (2013).
- [8] F. J. Gijsen, F. N. van de Vosse, J. Janssen, The influence of the non-newtonian properties of blood on the flow in large arteries: steady flow in a carotid bifurcation model, *Journal of biomechanics* 32 (6) (1999) 601–608.
- [9] A. Waele, *Viscometry and plastometry*, Oil and Colour Chemists' Association, 1923.
- [10] W. Ostwald, Ueber die geschwindigkeitsfunktion der viskosität disperser systeme. i, *Kolloid-Zeitschrift* 36 (2) (1925) 99–117.
- [11] P. J. Carreau, Rheological equations from molecular network theories, *Transactions of the Society of Rheology* 16 (1) (1972) 99–127.
- [12] S. Matsuhisa, R. B. Bird, Analytical and numerical solutions for laminar flow of the non-newtonian ellis fluid, *AIChE Journal* 11 (4) (1965) 588–595.
- [13] M. M. Cross, Rheology of non-newtonian fluids: a new flow equation for pseudoplastic systems, *Journal of colloid science* 20 (5) (1965) 417–437.
- [14] K. Yasuda, Investigation of the analogies between viscometric and linear viscoelastic properties of polystyrene fluids, Ph.D. thesis, Massachusetts Institute of Technology (1979).
- [15] M. T. Gallagher, R. A. Wain, S. Dari, J. P. Whitty, D. J. Smith, Non-identifiability of parameters for a class of shear-thinning rheological models, with implications for haematological fluid dynamics, *Journal of Biomechanics* 85 (2019) 230–238.

- [16] V. Mazzanti, F. Mollica, N. El Kissi, Rheological and mechanical characterization of polypropylene-based wood plastic composites, *Polymer Composites* 37 (12) (2016) 3460–3473.
- [17] S. Bair, A more complete description of the shear rheology of high-temperature, high-shear journal bearing lubrication, *Tribology transactions* 49 (1) (2006) 39–45.
- [18] B. E. Meza, J. M. Peralta, S. E. Zorrilla, Effect of temperature and composition on rheological behaviour and sagging capacity of glaze materials for foods, *Food Hydrocolloids* 117 (2021) 106689.
- [19] G. Santesarti, M. Marino, F. Viola, R. Verzicco, G. Vairo, A quasi-analytical solution for “carreau-yasuda-like” shear-thinning fluids flowing in slightly tapered pipes, *Journal of Non-Newtonian Fluid Mechanics*, (submitted) [arXiv:2502.14991](https://arxiv.org/abs/2502.14991) (2025).
- [20] M. Itskov, et al., *Tensor algebra and tensor analysis for engineers*, Springer, 2007.
- [21] F. Irgens, *Rheology and non-newtonian fluids*, Vol. 190, Springer, 2014.
- [22] Y. Zare, S. P. Park, K. Y. Rhee, Analysis of complex viscosity and shear thinning behavior in poly (lactic acid)/poly (ethylene oxide)/carbon nanotubes biosensor based on carreau–yasuda model, *Results in Physics* 13 (2019) 102245.
- [23] M. Ohta, E. Iwasaki, E. Obata, Y. Yoshida, Dynamic processes in a deformed drop rising through shear-thinning fluids, *Journal of non-newtonian fluid mechanics* 132 (1-3) (2005) 100–107.
- [24] Y. Pratumwal, W. Limtrakarn, S. Muengtaweepongsa, P. Phakdeesan, S. Duangburong, P. Eiamaram, K. Intharakham, Whole blood viscosity modeling using power law, casson, and carreau yasuda models integrated with image scanning u-tube viscometer technique., *Songklanakarin Journal of Science & Technology* 39 (5) (2017).

- [25] C. Colosi, S. R. Shin, V. Manoharan, S. Massa, M. Costantini, A. Barbetta, M. R. Dokmeci, M. Dentini, A. Khademhosseini, Microfluidic bioprinting of heterogeneous 3d tissue constructs using low-viscosity bioink, *Advanced materials* 28 (4) (2016) 677–684.
- [26] K. A. Aho, *Foundational and applied statistics for biologists using R*, CRC Press, 2013.
- [27] F. Chirianni, G. Vairo, M. Marino, Influence of extruder geometry and bio-ink type in extrusion-based bioprinting via an in silico design tool, *Meccanica* 59 (8) (2024) 1285–1299.
- [28] F. Chirianni, G. Vairo, M. Marino, Development of process design tools for extrusion-based bioprinting: From numerical simulations to nomograms through reduced-order modeling, *Computer Methods in Applied Mechanics and Engineering* 419 (2024) 116685.
- [29] M. Conti, G. Santesarti, F. Scocozza, M. Marino, Models and simulations as enabling technologies for bioprinting process design, in: *Bioprinting*, Elsevier, 2022, pp. 137–206.